JLAB-THY-96-05

Jefferson Lab

The Thomas Jefferson National Accelerator Facility
Theory Group Preprint Series

Additional copies are available from the authors.

The Southeastern Universities Research Association (SURA) operates the Thomas Jefferson National Accelerator Facility for the United States Department of Energy under contract DE-AC05-84ER40150.

Light-cone quark model predictions for radiative meson decays

H.M. Choi[a,b] and Chueng-Ryong Ji[a]

[a] *Department of Physics, North Carolina State University, Raleigh, N.C. 27695-8202, USA*

[b] *CEBAF, 12000 Jefferson Avenue, Newport News, Virginia, 23606*

Abstract

We investigate the radiative decays of pseudoscalar (π, K, η, η'), vector$(\rho, K^*, \omega, \phi)$ and axial vector (A_1) mesons using a simple relativistic constituent quark model. For both simplicity and relativity, we take advantage of the distinguished features in the light-cone quantization method; (1) the Fock-state expansion of meson wavefunctions are not contaminated by the vacuum fluctuation, (2) the problem of assigning quantum numbers J^{PC} to mesons is circumvented by the Melosh transformation. Except the well-known constituent quark masses of (u,d,s) quarks and the spin-averaged meson masses, the only parameter in the model is the gaussian parameter β which determines the broadness(or sharpness) of radial wavefunction. Our overall predictions of pseudoscalar, vector and axial vector meson radiative decay processes are remarkably in a good agreement witb the experimental data.

I. INTRODUCTION

While the nonperturbative QCD methods such as QCD sum-rule techniques [1–3] and lattice QCD calculations [4–6] are available, there is still growing interest in using simple relativistic quark models [7–12] to describe hadron properties. Our relativistic quark model [7,8] is based upon the Fock state decomposition of hadronic state which arises naturally in the 'light-cone quantization' of QCD. In this approach, a hadron is characterized by a set of Fock state wave functions, the probability amplitudes for finding different combinations of bare quarks and gluons in the hadron at a given light-cone time $\tau = t + z/c$. These wave functions provided the essential link between hadronic phenomena at short distances(perturbative) and at long distances(non-perturbative) [13].

The distinguished features in the light-cone approach are the simplicity of the vacuum except the zero modes and the dynamical property of rotation operators. The vacuum at equal τ has dramatic difference compare to the vacuum at equal t. For the particle which has the mass m and the four-momentum $k = (k^0, k^1, k^2, k^3)$, the relativistic energy-momentum relation at equal τ is given by

$$k^- = \frac{\mathbf{k}_{\perp i}^2 + m^2}{k^+}, \tag{1.1}$$

where the light-cone energy conjugate to τ is given by $k^- = k^0 - k^3$ and the light-cone momenta $k^+ = k^0 + k^3$ and $\mathbf{k}_\perp = (k^1, k^2)$ are orthogonal to k^- and form the light-cone three-momentum $\underline{k} = (k^+, \mathbf{k}_\perp)$. The rational relation given by Eq.(1) is drastically different from the irrational energy-momentum relation at equal t given by

$$k^0 = \sqrt{\mathbf{k}^2 + m^2}, \tag{1.2}$$

where the energy k^0 is conjugate to t and the three-momentum vector $\mathbf{k}$ is given by $\mathbf{k} = (k^1, k^2, k^3)$. The important point here is that signs of k^+ and k^- are correlated while at equal t the signs of k^0 and $\mathbf{k}$ are not correlated. Thus the momentum k^+ is always positive because only the positive energy k^- makes the system evolve to the future direction(*i.e.* positive τ), while the momentum k^3 can be either positive or negative even though k^0 is positive to evolve the system in the future direction(*i.e.* positive t). This provides a remarkable feature to the light-cone vacuum, namely , the Fock state vacuum is an eigenstate of the full Hamiltonian. Consequently, all bare quanta in an hadronic Fock state are associated with the hadron and none are disconnected elements of the vacuum [13].

Furthermore, the problem of boost operators at equal t changing particle numbers can be cured by this framework since the quantization surface $\tau = 0$ is invariant under both longitudinal and transverse boosts defined at equal τ. However, the quantization surface $\tau = 0$ is not invariant under the transverse rotation whose direction is perpendicular to the direction of the quantization axis z at equal τ [14]. Thus, the transverse angular momentum operator involves the interaction that changes the particle number and it is not easy to specify the total angular momentum of a particular hadronic state. Also τ is not invariant under parity [15]. We circumvent these problems by using the Melosh transformation of each constituents from equal t to equal τ.

The key approximation in the light-cone approach is the mock-hadron approximation [16] to saturate the Fock state expansion by the constituent quark and anti-quark and treat the saturated constituent Fock state as a free state as far as the spin-orbit part is concerned while the radial part is given by the ground state of the harmonic oscillator wavefunction. Then, the assignment of the quantum numbers such as angular momentum, parity and charge conjugation to the light-cone wavefunctions is given by the Melosh transformation [17]. For example, the meson state $|M>$ is represented by

$$|M>= \Psi_{Q\bar{Q}}^M |Q\bar{Q}>, \tag{1.3}$$

where Q and $\bar{Q}$ are the effective dressed quark and antiquark. The model wavefunction is then given by [7,8]

$$\Psi_{Q\bar{Q}}^M = \Psi_M(x_i, \mathbf{k}_{\perp i}, \lambda_i) = \Phi_M(x_i, \mathbf{k}_{\perp i}) \chi_M(x_i, \mathbf{k}_{\perp i}, \lambda_i) \tag{1.4}$$

where the radial wavefunction is given by

$$\Phi_M(x_i, \mathbf{k}_{\perp i}) = A \exp\Big[-\sum_{i=1}^{2} \frac{\mathbf{k}_{\perp i}^2 + m_i^2}{x_i} / 8\beta^2\Big], \tag{1.5}$$

and the spin-orbit wavefunction $\chi_M(x_i, \mathbf{k}_{\perp i}, \lambda_i)$ is obtained by the interaction independent Melosh transformation from the ordinary equal-time static spin-orbit wavefunction assigned by the quantum numbers J^{PC}. These wavefunctions are represented by the Lorentz-invariant variables $x_i = p_i^+ / P^+$, $\mathbf{k}_{\perp i} = \mathbf{p}_{\perp i} - x_i \mathbf{P}_\perp$, and λ_i, where $P^\mu = (P^+, P^-, \mathbf{P}_\perp) = (P^0 + P^3, (m_M^2 + \mathbf{P}_\perp{}^2)/P^+, \mathbf{P}_\perp)$ is the momentum of the meson M, and p_i^μ and λ_i are the momentum and the helicity of constituent quarks, respectively. Then, the light-cone spin-orbit wavefunction corresponding to the specific quantum number J^{PC} is given by

$$\chi_M(x_i, \mathbf{k}_{\perp i}, \lambda_i) = \bar{u}_{\lambda_1} \Gamma_{M,\mu} v_{\lambda_2}, \tag{1.6}$$

where the operators $\Gamma_{M,\mu}$ are given by [8]

$$J^{PC} = 0^{-+}; \Gamma_p = (m_p + P)\gamma_5, \tag{1.7}$$

$$1^{--}; \Gamma_{v,\mu} = m_v \not\epsilon(\mu) + \frac{[P, \not\epsilon(\mu)]}{2}, \tag{1.8}$$

$$1^{++}; \Gamma_{a,\mu} = (m_a + P)\Big[\frac{k \cdot P}{m_a} \not\epsilon(\mu) + \frac{[\not\epsilon(\mu), \not k]}{2}\Big] \gamma_5. \tag{1.9}$$

Here the space components $\vec{\epsilon}(\mu)$ of the polarization four-vectors $\epsilon(\mu)$ in the rest frame have the components $\vec{\epsilon}(\pm) = \mp(1, \pm i, 0)/\sqrt{2}$, $\vec{\epsilon}(0) = (0, 0, 1)$.

Using this model wavefunction Eq.(1.4), we have calculated various static properties of π, K, ρ, and A_1 mesons [7,8]. Since our model provided a remarkably good description of static properties for the pion and K-mesons and reproduced the basic features of the lattice QCD and the QCD sum-rule results for π, K, ρ, and A_1 mesons [7,8], it is of our interest to investigate more observables with the same model. In this paper, we present a comprehensive study of the radiative decays of pseudoscalar(π, K, η, η'), vector(ρ, K^*, ω, ϕ) and axial vector(A_1) mesons.

Both in the past works and the present work, we use the spin averaged mass as argued by Dziembowski [9,10]. Before we perform the Melosh transformation, we assume that the starting ground state mesons are described by the harmonic oscillator wavefunctions. These equal t wavefunctions are known to give a reasonable first approximation of the static properties [18]. Since these starting wavefunctions prior to the Melosh transformation are valid in a scheme without short-range hyperfine interactions, it is reasonable to assume the spin averaged mass [9]. The spin averaged masses of π, K, ρ, and A_1 mesons are given by [7,8] $m_\pi = m_\rho = 0.612$ GeV, $m_K = m_{K^*} = 0.793$ GeV and $m_{A_1} = 1.120$ GeV. Since we consider now η, η', ω and ϕ mesons also in this work, we present the details of how we obtain the spin averaged values of η, η', ω and ϕ mesons in the Appendix A. The flavor assignment of η and η' mesons in the quark and antiquark basis are as follows:

$$\eta = X_\eta \frac{(u\bar{u} + d\bar{d})}{\sqrt{2}} - Y_\eta s\bar{s}, \tag{1.10}$$

$$\eta' = X_{\eta'} \frac{(u\bar{u} + d\bar{d})}{\sqrt{2}} + Y_{\eta'} s\bar{s}, \tag{1.11}$$

where $X_\eta = Y_{\eta'} = -\sin\theta_{P_S}$ and $Y_\eta = X_{\eta'} = \cos\theta_{P_S}$ with $\theta_{P_S} = \theta_{SU(3)} - \theta_{ideal} \approx \theta_{SU(3)} - 35^\circ$. Of particular interest are the values of mixing angle $\theta_{SU(3)} = -10^\circ$(so called "perfect mixing") [19,20] and -23° that are used in our analysis. The spin averaged masses of η and η' for each scheme are given in Table I. For ω and ϕ mesons, we use the scheme of ideal

mixing [21] and obtain the spin averaged masses $m_\omega = 928$ MeV and $m_\phi = 799$ MeV. Once the spin averaged masses are fixed, then besides the well-known constituent quark masses of (u,d,s) quarks,*i.e.* $m_u = m_d = 330$ MeV and $m_s = 450$ MeV, the only papameter in this model is the gaussian parameter β which determines the broadness(or sharpness) of radial wavefunction. We will present our numerical results for a typical β value of $\beta = 360$ MeV throughout the paper, unless stated otherwise. The predictions for other values of β are summarized in Table II.

In the following section, Sec.II, we calculate the form factors, charge radii, magnetic and quadrupole moments of the ρ and A_1 mesons and compare with the results of QCD sum rules [22]. In Sec.III, the transition form factors and the decay widths of the transitions $V \to P_S\gamma^*$, $P_S \to V\gamma^*$ ($V = \rho, K^*, \omega, \phi$ and $P_S = \pi, K, \eta, \eta'$) and $A_1 \to \pi\gamma^*$ are presented including the comparison with other theoretical results as well as the experimental data. In Sec.IV, we present the calculation of the transition form factors of the $\pi^0 \to \gamma^*\gamma$, $\eta \to \gamma^*\gamma$ and $\eta' \to \gamma^*\gamma$ transitions and compare our results with the recent experimental data [23–25]. Summary and discussions of our major results are followed in Sec.V. In the Appendix A, the details of how we obtain the spin averaged masses of η, η', ω and ϕ are presented. In the Appendix B, we present the derivation of the formula used for the electromagnetic decay widths.

II. THE FORM FACTORS OF THE ρ AND $A1$ MESONS

A. The ρ meson form factors.

Our analysis will be carried out using the standard light-cone frame(LCF)($q^\pm = q^0 \pm q^3$) [26]:

$$P = (P^+, P^-, \mathbf{P}_\perp) = (P^+, \frac{M^2}{P^+}, \mathbf{0}_\perp),$$

$$q = (q^+, q^-, \mathbf{q}_\perp) = (0, \frac{Q^2}{P^+}, \mathbf{q}_\perp), \tag{2.1}$$

where M is the meson mass and the photon momentum is transverse to the direction of the incident spin-one system, with $q_\perp^2 = Q^2 = -q^2$.

The Lorentz invariant electromagnetic form factors $F_i (i = 1, 2, 3)$ for a spin 1 particle are defined [27] by the matrix elements of the current operator J^μ between the initial $|P, \lambda>$ and the final $|P', \lambda'>$ eigenstate of momentum P and helicity λ as follows:

$$< P',\lambda'|J^\mu|P,\lambda > = \epsilon'^*_\alpha \epsilon_\beta \Big[- g^{\alpha\beta}(P+P')^\mu F_1(Q^2) + (g^{\mu\beta}q^\alpha - g^{\mu\alpha}q^\beta)F_2(Q^2) + q^\alpha q^\beta (P+P')^\mu F_3(Q^2)/(2M^2)\Big], \quad (2.2)$$

where $q = P' - P$ and the polarization vectors of the initial and final mesons $\epsilon \equiv \epsilon_\lambda$ and $\epsilon' \equiv \epsilon_{\lambda'}$, respectively, are defined by

$$\epsilon(0) = \frac{1}{M}(P^+, -\frac{M^2}{P^+}, \mathbf{0}_\perp), \quad \epsilon'(0) = \frac{1}{M}(P^+, \frac{-M^2+Q^2}{P^+}, \mathbf{q}_\perp),$$
$$\epsilon(\pm 1) = \frac{\mp 1}{\sqrt{2}}(0, 0, 1, \pm i), \quad \epsilon'(\pm 1) = \frac{\mp 1}{\sqrt{2}}(0, \frac{2\mathbf{q}_\perp}{P^+}, 1, \pm i). \quad (2.3)$$

Also, the Lorentz invariant form factors $F_i(Q^2)$ are related to the charge, magnetic and quadrupole form factors of a meson [27] as follows:

$$F_C = F_1 + \frac{2}{3}\kappa F_Q,$$
$$F_M = F_2,$$
$$F_Q = F_1 - F_2 + (1+\kappa)F_3, \quad (2.4)$$

where $\kappa = Q^2/4M^2$ is a kinematic factor. At zero momentum transfer,these form factors are proportional to the usual static quantities of charge e, magnetic moment μ_1, and quadrupole moment Q_1:

$$F_C(0) = 1, \quad eF_M(0) = 2M\mu_1, \quad eF_Q(0) = M^2 Q_1. \quad (2.5)$$

In the light-cone quark model, the matrix element can be calculated by the convolution of initial and final light-cone wavefunctions of a meson:

$$< P',\lambda'|J^\mu|P,\lambda > = e_1 \int_0^1 dx \int \frac{d^2\mathbf{k}_\perp}{16\pi^3} \Phi_M(x, \mathbf{k}_\perp + (1-x)\mathbf{q}_\perp)\Phi_M(x, \mathbf{k}_\perp) \times \sum_{\lambda,\lambda'} \chi^\dagger_{\lambda'_1,\lambda'_2}(x, \mathbf{k}_\perp + (1-x)\mathbf{q}_\perp)\Gamma^\mu \chi_{\lambda_1,\lambda_2}(x, \mathbf{k}_\perp) + e_2(1 \leftrightarrow 2 \text{ of the first term}), \quad (2.6)$$

where the spin covariant functions $\chi(x, \mathbf{k}_\perp)$ are given by Eqs.(1.7)-(1.9) and the vertex Γ^μ is obtained from the expression $\frac{\bar{u}(p')}{(p'^+)^{1/2}}\gamma^\mu \frac{u(p)}{(p^+)^{1/2}}$ [28].

The relationship in Eq.(2.2) between the covariant form factors and current matrix elements can be applied [29,30], in principle, to any choice of Lorentz frame. As discussed by Brodsky and Hiller [31], in the standard LCF [26], $q^+ = 0$, $q_y = 0$, $q_x = Q$, the three form factors can be obtained from the '+'-component of three helicity matrix elements:

$$F_C = \frac{1}{2P^+(2\kappa+1)}\Big[\frac{16}{3}\kappa\frac{F^+_{+0}}{\sqrt{2\kappa}} - \frac{2\kappa-3}{3}F^+_{00} + \frac{2}{3}(2\kappa-1)F^+_{+-}\Big],$$
$$F_M = \frac{2}{2P^+(2\kappa+1)}\Big[(2\kappa-1)\frac{F^+_{+0}}{\sqrt{2\kappa}} + F^+_{00} - F^+_{+-}\Big],$$
$$F_Q = \frac{1}{2P^+(2\kappa+1)}\Big[2\frac{F^+_{+0}}{\sqrt{2\kappa}} - F^+_{00} - \frac{\kappa+1}{\kappa}F^+_{+-}\Big]. \quad (2.7)$$

where we defined $< P',\lambda'|J^\mu|P,\lambda > \equiv F^\mu_{\lambda'\lambda}$. After a tedious but straightforward calculation, we find the following expressions for the helicity form factors of the ρ meson:

$$F^+_{00} = N_\rho \int_0^1 \frac{dx}{x(1-x)} \exp[-\frac{\xi^2 + \tilde{m}_1^2 + x(\tilde{m}_2^2 - \tilde{m}_1^2)}{x(1-x)}] \times \Big[2x^2(1-x)^2 + x(1-x)(a_1^2+a_2^2) + (a_1a_2)^2 - (a_1^2+a_2^2-4a_1a_2)\xi^2 + \xi^4\Big], \quad (2.8)$$

$$F^+_{+0} = \frac{Q}{2\sqrt{2}\beta}N_\rho \int_0^1 \frac{dx}{x}\exp[-\frac{\xi^2 + \tilde{m}_1^2 + x(\tilde{m}_2^2 - \tilde{m}_1^2)}{x(1-x)}](a_1 - a_2)[a_1a_2 - \xi^2 - x(1-x)], \quad (2.9)$$

$$F^+_{+-} = -\frac{Q^2}{4\beta^2}N_\rho \int_0^1 \frac{(1-x)dx}{x} a_1a_2 \exp[-\frac{\xi^2 + \tilde{m}_1^2 + x(\tilde{m}_2^2 - \tilde{m}_1^2)}{x(1-x)}], \quad (2.10)$$

where

$$\xi^2 = \frac{(1-x)^2Q^2}{16\beta^2}, \quad \tilde{m}_i = \frac{m_i}{2\beta},$$
$$a_1 = \frac{(xm_\rho + m_1)}{2\beta}, \quad a_2 = \frac{((1-x)m_\rho + m_2)}{2\beta}, \quad (2.11)$$

and m_1,m_2 are the constituent masses of the quark and anti-quark. The normalization constant $N_\rho = (\frac{4A_\rho\beta^3}{\pi P^+})^2$ is fixed by the definition of charge, $F_C(0) = 1$. For the systems of spin 1 or greater, in addition to the parity and time-reversal invariance of the current operator $J^+(0)$ [27,31], an additional constraint on the current operator comes from the rotational covariance requirement [29,32,33]. The angular condition for the spin 1 system is given by [32–34]:

$$\Delta(Q^2) = (1+2\kappa)F^+_{++} + F^+_{+-} - \sqrt{8\kappa}F^+_{+0} - F^+_{00} = 0. \quad (2.12)$$

As a matter of fact, the expressions of right-hand side in Eq.(2.7) are thus not unique because of the angular condition in Eq.(2.12). As pointed out by Refs. [33,34], unless the exact Poincaré covariant current operator beyond one-body sector is used, the angular condition is in general violated(i.e., $\Delta(Q^2) \neq 0$) and the calculation of the form factors F_i is dependent on the expressions of the r.h.s. of Eq.(2.7). Examples of different choices of current combinations can be found in Ref. [34] for the calculation of ρ meson form factors.

As shown in Fig.1(a), our result obtained for $\Delta(Q^2)$ is comparable with other choices given in Ref. [34].

The magnetic(in unit of $e/2M$) and quadrupole moments(in unit of e/M^2) of the ρ meson are obtained by Eq.(2.5);

$$\mu_1 = 2.1, \quad Q_1 = 0.41. \tag{2.13}$$

These values are not much different from the values of other model predictions presented in Ref. [34]($\mu_1 = 2.26$, $Q_1 = 0.37$) and Ref. [35]($\mu_1 = 2.3$, $Q_1 = 0.45$). We also calculated the electromagnetic radii associated with the form factors, F_C^ρ, F_M^ρ and F_Q^ρ as $< r_{F_C}^2 >=$ 14 GeV^{-2}, $< r_{F_M}^2 >=$ 22 GeV^{-2} and $< r_{F_Q}^2 >= -5$ GeV^{-2}, respectively. The results of $F_C(Q^2)$, $F_M(Q^2)$ and $F_Q(Q^2)$ for $0 \le Q^2 \le 5$ GeV^2 are shown in Fig.1(b). To see the effect of the Melosh transformation(the measure of relativistic effects), we calculated the charge form factor by turning the Melosh rotations off and included the result in Fig.1(b). The charge radius from this nonrelativistic form fator is $< r^2 >_{\text{non-rel}} = 10.6$ GeV^{-2} which is about 30% smaller than that of relativistic charge radius. In Fig.1(c), we also compared our results with the previous calculations of these form factors which were made in the framework of QCD sum rules by Ioffe and Smilga [22] [1].

B. The $A1$ meson form factors.

The electromagnetic form factors of the $A1$ meson are defined by Eq.(2.2) as in the case of the ρ meson. Using the similar method taken in the ρ meson case, we find the following helicitiy component of the $A1$ form factors analogous to Eqs.(2.8)-(2.10);

$$F_{00}^+ = N_{A1}\int_0^1 \frac{dx}{x(1-x)}\exp[-\frac{\xi^2+\tilde{m}_1^2+x(\tilde{m}_2^2-\tilde{m}_1^2)}{x(1-x)}]\Big[6x^3(1-x)^3+2x^2(1-x)^2$$
$$[\ a_1^2+a_2^2-\xi^2]+x(1-x)[(a_1a_2)^2+\xi^4]-\xi^2[(a_1a_2)^2-(a_1^2+a_2^2+4a_1a_2)\xi^2+\xi^4]\Big], \tag{2.14}$$

$$F_{+0}^+ = \frac{Q}{2\beta}N_{A1}\int_0^1 \frac{dx}{x}\exp[-\frac{\xi^2+\tilde{m}_1^2+x(\tilde{m}_2^2-\tilde{m}_1^2)}{x(1-x)}](a_2-a_1)\Big[2x^2(1-x)^2$$
$$+x(1-x)(4\xi^2-a_1a_2)+\xi^4-a_1a_2\xi^2\Big], \tag{2.15}$$

[1]The definition of the form factors(G_i) by QCD sum-rule [22] and the definition in this paper are related as follows: $G_1 = F_1$, $G_2 = F_2 - F_1$ and $G_3 = F_3/2$

$$F_{+-}^+ = \frac{Q^2}{8\beta^2}N_{A1}\int_0^1 \frac{(1-x)dx}{x}\exp[-\frac{\xi^2+\tilde{m}_1^2+x(\tilde{m}_2^2-\tilde{m}_1^2)}{x(1-x)}](a_2-a_1)^2[x(1-x)+\xi^2]. \tag{2.16}$$

As one can see in Fig.2(a), the behavior of each form factor looks similar to the ρ meson case. In Fig.2(a), we also included $|\Delta(Q^2)|$ for A_1. The amount of deviation from the rotational covariance is almost same as that of the ρ meson case.

The electromagnetic radii associated with $F_C^{A_1}$, $F_M^{A_1}$ and $F_Q^{A_1}$ are obtained as $< r_{F_C}^2 >=$ 10 GeV^{-2}, $< r_{F_M}^2 >=$ 20 GeV^{-2} and $< r_{F_Q}^2 >= -10$ GeV^{-2}, respectively. The magnetic and quadrupole moments of the A_1 meson are also obtained as

$$\mu_1 = 2.16, \quad Q_1 = 1.34. \tag{2.17}$$

While the magnetic moment of A_1 does not differ from that of the ρ meson, the quadrupole moment of A_1 is about 4 times greater than that of the ρ meson in accordance with the fact that the A_1 meson is a bound state with nonzero orbital angular momentum $l = 1$ [35]. In Fig.2(b), we compare our results with those of QCD sum rules [22].

III. THE TRANSITION FORM FACTORS OF $V \to P_S\gamma^*$, $\eta' \to \rho(\omega)\gamma^*$, AND $A_1 \to \pi\gamma^*$

The transition form factors of $A \to B\gamma^*$ ($(A,B) = (\rho,\pi),(\rho,\eta),(\omega,\pi),(\omega,\eta),(K^*,K)$, $(\eta',\rho),(\eta',\omega),(\phi,\eta),(\phi,\eta')$) and $A_1 \to \pi\gamma^*$ are defined by

$$< B(P')|J^\mu|A(P,\lambda) > = eG_{AB}(Q^2)\epsilon^{\mu\nu\alpha\beta}\epsilon_\nu(P,\lambda)P'_\alpha P_\beta, \tag{3.1}$$

$$< \pi(P')|J^\mu|A_1(P,\lambda) > = \frac{e}{m_{A_1}}\Big[(\mathcal{P}\cdot q g^{\mu\nu}-\mathcal{P}^\mu q^\nu)G_1(Q^2)$$
$$+\frac{1}{m_{A_1}^2}(\mathcal{P}\cdot q q^\mu - q^2\mathcal{P}^\mu)q^\nu G_2(Q^2)\Big]\epsilon_\nu(P,\lambda), \tag{3.2}$$

where $\epsilon(P,\lambda)$ denotes the polarization vector of the initial particles and $\mathcal{P} = P + P'$. As shown in the Appendix B, the width of the decay $A \to B\gamma$ is given by

$$\Gamma(A \to B\gamma) = \frac{\alpha}{2S_A+1}|G_{AB}(0)|^2(\frac{M_A^2-M_B^2}{2M_A})^3, \tag{3.3}$$

where α is the fine structure constant, S_A is the spin of the initial particle and $M_{A(B)}$ is the mass[2] of the meson A(B). In the case of $A_1 \to \pi\gamma$ transition, the decay width is expressed

[2]This must be the physical mass rather than the spin-averaged mass because the phase factor is nothing to do with the model. Spin-averaged masses are used only for the calculation of form

in terms of $G_1(0)$(see Appendix B);

$$\Gamma(A_1 \to \pi\gamma) = \frac{4\alpha}{3}|\frac{G_1(0)}{M_{A_1}}|^2(\frac{M_{A_1}^2 - M_\pi^2}{2M_{A_1}})^3. \tag{3.4}$$

Carrying out again a tedius but straightforward calculation, we find the following expressions for the form factors $G_{\rho\pi}(Q^2)$ and $G_{\omega\pi}(Q^2)$:

$$\begin{aligned} G_{\rho\pi}(Q^2) &= (e_u + e_d)I_1(m_M, m_q, \beta), \\ G_{\omega\pi}(Q^2) &= (e_u - e_d)I_1(m_M, m_q, \beta), \end{aligned} \tag{3.5}$$

where

$$\begin{aligned} I_1(m_M, m_q, \beta) = \frac{1}{2\beta}\sqrt{\frac{N_M N_\pi}{2}} \int_0^1 \frac{dx}{x} \exp[-\frac{\xi^2 + \tilde{m}_1^2 + x(\tilde{m}_2^2 - \tilde{m}_1^2)}{x(1-x)}] \\ \times \Big[a_1^i + a_2^i + a_1^f + a_2^f][x(1-x) - \xi^2] + a_1^i a_2^i(a_1^f + a_2^f) \\ + a_1^f a_2^f(a_1^i + a_2^i)\Big], \end{aligned} \tag{3.6}$$

and $a^{i(f)} = (x m_{M_{i(f)}} + m_q)/2\beta$ with i and f meaning incident and outgoing mesons. The normalization constants of the ρ and π-mesons are given by $N_\pi = N_\rho/2 = 2(\frac{2A_{\pi(\rho)}\beta^3}{\pi^{3/4}})^2$.

We obtained the following prediction of decay widths of the $\rho^\pm(770) \to \pi^\pm\gamma$ and $\omega(782) \to \pi\gamma$ transitions;

$$\begin{aligned} \Gamma(\rho^\pm \to \pi^\pm\gamma) = 69 \text{ keV} \quad (\Gamma^{\rm exp}_{\rho^\pm\to\pi^\pm\gamma} = 68 \pm 8 \text{ keV}), \\ \Gamma(\omega \to \pi\gamma) = 708 \text{ keV} \quad (\Gamma^{\rm exp}_{\omega\to\pi\gamma} = 717 \pm 51 \text{ keV}). \end{aligned} \tag{3.7}$$

Our results for the decay widths $\Gamma_{\rho\pi}$ and $\Gamma_{\omega\pi}$ are in a very good agreement with the experimental data. The electromagnetic radii of these form factors are obtained as $< r^2_{G_{\rho\pi}} >= 7$ GeV^{-2} and $< r^2_{G_{\omega\pi}} >= 20$ GeV^{-2}, respectively. In Fig.3(a), we present the transition form factor of $\rho \to \pi\gamma^*$ for $0 \le Q^2 \le 8$ GeV^2 and compare with other model predictions of Refs. [34,36]. In Fig.3(b), our prediction(solid line) of $\omega \to \pi\gamma^*$ transition form factor in the space like region is compared with the VDM(dashed line) with $F_{\omega\pi} = 1/(1 + Q^2/M_\rho^2)$ and the pole fit(dotted line) of the experimental data in the time-like region [38,39].

Similarly, we calculated all other radiative decay processes between vector (1^{--}) and pseudoscalar mesons(0^{-+}) using the one loop integral formula $I_1(m_M, m_q, \beta)$ given by

---

factors.

Eq.(3.6). We needed to change only the spin-averaged meson masses m_M and constituent quark masses $m_i (i = 1, 2)$, accordingly. Thus, for the $\rho \to \eta\gamma^*$ and $\omega \to \eta\gamma^*$ decays, we obtain the following transition form factors

$$\begin{aligned} G_{\rho\eta}(Q^2) &= X_\eta(e_u - e_d)I_1(m_M, m_q, \beta), \\ G_{\omega\eta}(Q^2) &= X_\eta(e_u + e_d)I_1(m_M, m_q, \beta). \end{aligned} \tag{3.8}$$

Using the two different mixing schemes, *i.e.*, $\theta_{SU(3)} = -10^\circ$ and -23°, we obtain the decay widths of the transitions $\rho \to \eta\gamma$ and $\omega \to \eta\gamma$ as $\Gamma^{-10^\circ}_{\rho\to\eta\gamma} = 56$ keV, $\Gamma^{-10^\circ}_{\omega\to\eta\gamma} = 6.4$ keV and $\Gamma^{-23^\circ}_{\rho\to\eta\gamma} = 65$ keV, $\Gamma^{-23^\circ}_{\omega\to\eta\gamma} = 7.4$ keV, respectively. Both schemes are in excellent agreement with the experimental data of $\Gamma^{\rm exp}_{\rho\to\eta\gamma} = 58 \pm 10$ keV and $\Gamma^{\rm exp}_{\omega\to\eta\gamma} = 7.0 \pm 1.8$ keV. The electromagnetic charge radii of $\rho \to \eta\gamma^*$ transition are also predicted as $< r^2_{G_{\rho\eta}} >= 16$ GeV^{-2} for -10° and 18 GeV^{-2} for -23° mixing angle. The charge radii for $\omega \to \eta\gamma^*$ transition are $< r^2_{G_{\omega\eta}} >= 5$ GeV^{-2} for -10° and 6 GeV^{-2} for -23°, respectively.

The form factors of the $\eta' \to \rho\gamma^*$ and $\eta' \to \omega\gamma^*$ are given by

$$\begin{aligned} G_{\eta'\rho}(Q^2) &= X_{\eta'}(e_u - e_d)I_1(m_M, m_q, \beta), \\ G_{\eta'\omega}(Q^2) &= X_{\eta'}(e_u + e_d)I_1(m_M, m_q, \beta). \end{aligned} \tag{3.9}$$

Our predictions of the decay widths are given by $\Gamma^{-10^\circ}_{\eta'\to\rho\gamma} = 117$ keV, $\Gamma^{-10^\circ}_{\eta'\to\omega\gamma} = 9.7$ keV and $\Gamma^{-23^\circ}_{\eta'\to\rho\gamma} = 72$ keV, $\Gamma^{-23^\circ}_{\eta'\to\omega\gamma} = 6.0$ keV. The experimental data of $\Gamma^{\rm exp}_{\eta'\to\rho\gamma} = 61 \pm 8$ keV and $\Gamma^{\rm exp}_{\eta'\to\omega\gamma} = 5.9 \pm 0.9$ keV. It is interesting to note that in case of transitions involving η', the result of -23° mixing scheme is much better than that of -10° mixing scheme. The electromagnetic charge radii for -23° mixing angle are predicted as $< r^2_{G_{\eta'\rho}} >= 12$ GeV^{-2} and $< r^2_{G_{\eta'\omega}} >= 4$ GeV^{-2}, respectively.

The transitions of the $K^{*\pm} \to K^\pm\gamma^*$ and $K^0 \to K^0\gamma^*$ in which the constituent quarks have unequal masses are also interesting processes to test our model predictions. As shown in our previous works [7], the predictions for the kaon charge radius $< r^2_K >^{1/2}$, the kaon form factor F_K, and the decay constant f_K are consistent with available experimental data. The transition form factors of the charged and netural K^* decays are given by

$$\begin{aligned} G_{K^{*\pm}K^\pm}(Q^2) &= \pm(e_u + e_s)I_1(m_M, m_q, \beta), \\ G_{K^{*0}K^0}(Q^2 &= (e_d + e_s)I(m_M, m_q, \beta). \end{aligned} \tag{3.10}$$

Using the spin averaged masses of $m_{K^{*\pm}} = 792.1$ MeV and $m_{K^{*0}} = 796.5$ MeV and the constituent quark mass $m_s = 0.45$ GeV [7], we obtain the decay widths for these charged

and neutral vector kaon decay processes as $\Gamma_{K^{*\pm}\to K^{\pm}\gamma}$= 53 keV, $\Gamma_{K^{*0}\to K^{0}\gamma}$= 122 keV, respectively. The experimental data are $\Gamma^{\rm exp}_{K^{*\pm}\to K^{\pm}\gamma}$= 50 ± 5 keV, $\Gamma^{\rm exp}_{K^{*0}\to K^{0}\gamma}$= 117 ± 10 keV. The electromagnetic transition charge radii are predicted as $< r^2_{G_{K^{*\pm}K^{\pm}}} >$= 11 GeV^{-2} and $< r^2_{G_{K^{*0}K^{0}}} >$= 10 GeV^{-2}. In Fig.4, we reported Q^2-dependence of transition form factor of charged and neutral vector kaon,*i.e.*, $G_{K^{*+}K^{+}}(Q^2)$ and $G_{K^{*0}K^{0}}(Q^2)$, respectively, for $0 \le Q^2 \le 10$ GeV^2. Even though we showed the result of $\beta = 0.36$ GeV only, we note that our results become much closer to those of Bethe-Salpeter(BS) quark model prediction [39] with smaller values of β,*i.e.*, $\beta \sim 0.3$ GeV.

For the decay processes of $\phi \to \eta(\eta')\gamma^*$, the transition form factors of $\phi \to \eta\gamma^*$ and $\phi \to \eta'\gamma^*$ are given by

$$G_{\phi\eta}(Q^2) = Y_\eta 2e_s I_1(m_M, m_q, \beta)$$
$$G_{\phi\eta'}(Q^2) = Y_{\eta'} 2e_s I_1(m_M, m_q, \beta). \qquad (3.11)$$

As shown in the Appendix A, we obtain the spin averaged mass of ϕ-meson as m_ϕ = .799 GeV. Our predictions of the decay widths of the transitions $\phi \to \eta\gamma$ and $\phi \to \eta'\gamma$ with $\theta_{SU(3)} = -10^\circ$ and -23° are given by $\Gamma^{-10^\circ}_{\phi\to\eta\gamma}$ = 61 keV, $\Gamma^{-10^\circ}_{\phi\to\eta'\gamma}$ = 0.28 keV and $\Gamma^{-23^\circ}_{\phi\to\eta\gamma}$ = 45 keV, $\Gamma^{-23^\circ}_{\phi\to\eta'\gamma}$ = 0.45 keV, respectively. The current experimental data are $\Gamma^{\rm exp}_{\phi\to\eta\gamma} = 56.9 \pm 2.9$ keV and $\Gamma^{\rm exp}_{\phi\to\eta'\gamma} < 1.8$ keV. It will be very interesting to compare our results, especially for $\phi \to \eta'\gamma$, with the more precise measurements envisioned at TJNAF. The electromagnetic charge radii for -10° mixing angle are also predicted as $< r^2_{G_{\phi\eta}} >$= 5 GeV^{-2} and $< r^2_{G_{\phi\eta'}} >$= 5.5 GeV^{-2}.

In the case of transition $A_1 \to \pi\gamma^*$, the kinematical factors in front of the form factor G_2 in Eq.(3.2) yields zero for a certain $\mathbf{q}_1^2$ in the standard Drell-Yan frame($\mathbf{P}_\perp = 0, q^+ = 0$) as discussed in Ref. [35]. This leads to a technical difficulty in extracting the form factors numerically from Eq.(3.2). Thus, as pointed out in Ref. [35], we use the following symmetric coordinate frame for the calculation of of $A_1 \to \pi\gamma^*$ transition form factors;

$$P = (P^+, \frac{m^2_{A_1} + \frac{1}{4}\mathbf{q}_1^2}{P^+}, -\frac{1}{2}\mathbf{q}_\perp), \quad P' = (P^+, \frac{m^2_\pi + \frac{1}{4}\mathbf{q}_1^2}{P^+}, \frac{1}{2}\mathbf{q}_\perp),$$
$$q = (0, \frac{m^2_\pi - m^2_{A_1}}{P^+}, \mathbf{q}_\perp). \qquad (3.12)$$

Then, we find the following expressions for the A_1 form factors:

$$G_1(Q^2) = \frac{m^2_{A_1}}{P^+(m^2_\pi - m^2_{A_1})}\left[G_0^+ + \frac{(m^2_\pi - m^2_{A_1} + Q^2)}{\sqrt{2}m_{A_1}}\frac{G_+^+}{Q}\right], \qquad (3.13)$$

$$G_2(Q^2) = \frac{2m^4_{A_1}}{(m^2_{A_1} - m^2_\pi)^2 Q}\left[G_0^x - \frac{(m^2_\pi - m^2_{A_1})}{2\sqrt{2}m_{A_1}P^+}G_+^+\right], \qquad (3.14)$$

where $G^\mu_\lambda \equiv < \pi(P')|J^\mu|A_1(P,\lambda) >$ and its matrix elements are given by

$$G_+^+ = \frac{Q}{2\beta}\sqrt{\frac{N_{A_1}N_\pi}{2}}\int_0^1 \frac{dx}{x}\exp[-\frac{\xi^2 + \tilde{m}_1^2 + x(\tilde{m}_2^2 - \tilde{m}_1^2)}{x(1-x)}](a_1^f + a_2^f)(a_1^i - a_2^i)[x(1-x) + \xi^2], \quad (3.15)$$

$$G_0^+ = \sqrt{2N_{A_1}N_\pi}\int_0^1 \frac{dx}{x(1-x)}\exp[-\frac{\xi^2 + \tilde{m}_1^2 + x(\tilde{m}_2^2 - \tilde{m}_1^2)}{x(1-x)}]\mathcal{G}_0, \qquad (3.16)$$

$$G_0^x = \frac{Q}{P^+}\sqrt{\frac{N_{A_1}N_\pi}{2}}\int_0^1 \frac{dx}{x^2}\exp[-\frac{\xi^2 + \tilde{m}_1^2 + x(\tilde{m}_2^2 - \tilde{m}_1^2)}{x(1-x)}]\mathcal{G}_0, \qquad (3.17)$$

with a common facfor $\mathcal{G}_0$ in the longitudinal component of G:

$$\mathcal{G}_0 = 2x^2(1-x)^2[(a_1^f + a_2^f) - (a_1^i + a_2^i)] + x(1-x)[a_1^f a_2^f(a_1^i + a_2^i) - a_1^i a_2^i(a_1^f + a_2^f)]$$
$$- \xi^4[(a_1^i + a_2^i) + (a_1^f + a_2^f)] + \xi^2[a_1^i a_2^i(a_1^f + a_2^f) + a_1^f a_2^f(a_1^i + a_2^i)]. \qquad (3.18)$$

In Fig.5, we show the result of A_1 transition form factors, $G_1(Q^2)$(solid line) and $G_2(Q^2)$(dashed line). While the form factor $G_2(Q^2)$ agrees with the predictions of the QCD sum-rules(dot-dashed line) [22] in the region $1 \le Q^2 \le 3$ GeV^2, the form factor $G_1(Q^2)$ seems to be quite different from the QCD sum-rule result(dotted line) [22]. However, there are other QCD sum rule calculations of G_1 and G_2 [40,41] and the results are rather different from each other. The authors of QCD sum-rules [22] also pointed out that their predictions for the transition $A_1 \to \pi\gamma^*$ are of semiqualitative results. The electromagnetic radii corresponding to these form factors are evaluated as $< r^2_{G_1} >$= 15 GeV^{-2} and $< r^2_{G_2} >$= −30 GeV^{-2}, respectively.

The decay width of $A_1^+(1260) \to \pi^+\gamma$ is obtained from Eq.(3.4) as

$$\Gamma(A_1 \to \pi\gamma) = 705 \ \text{keV}. \qquad (3.19)$$

The prediction of VDM [42,43] is given by $\Gamma^{VDM}_{A_1\to\pi\gamma} = 1000 - 1500$ keV and the experimental value has been reported [44,45] as $\Gamma(A_1^+ \to \pi^+\gamma) = 640 \pm 246$ keV using the measurment of Primakoff production of the A_1 resonance. Thus, our predicted width is quite consistent with the corresponding experimental data. In Refs. [35,37], the same decay width was calculated using the invariant mass of A_1 meson instead of the spin averaged mass. Their results $\Gamma(A_1^+ \to \pi^+\gamma)$ = 319 keV [35] and 250 keV [37] seem to have rather large discrepancy from the experimental data.

IV. THE FORM FACTORS OF $\pi^0 \to \gamma^*\gamma$ $\eta \to \gamma^*\gamma$ AND $\eta' \to \gamma^*\gamma$ TRANSITIONS

The transition form factor of $P_S \to \gamma^*\gamma(P_S = \pi^0, \eta,$ and $\eta')$ is defined from the matrix element of electromagnetic current $\Gamma_\mu = < \gamma(P+q)|J_\mu|P_S(P) >$ as follows:

$$\Gamma_\mu = ie^2 G_{P_S\gamma}(Q^2)\epsilon_{\mu\nu\rho\sigma}P^\nu\epsilon^\rho q^\sigma, \tag{4.1}$$

where P and q are the momenta of the incident pseudoscalar meson and virtual photon, respectively, and ϵ is the polarization vector of the final (on-shell) photon.

The Q^2 dependent decay rate for $P_S \to \gamma^*\gamma$ is given by[2]

$$\Gamma_{P_S\to\gamma^*\gamma}(Q^2) = \frac{\pi}{4}\alpha^2 M_{P_S}^3 G_{P_S\gamma}^2(Q^2), \tag{4.2}$$

where M_{P_S} is the mass of $P_S = \pi^0, \eta$, and η'. Here, the decay width is given by $\Gamma_{P_S\to\gamma\gamma}$ at $Q^2 = 0$. If we choose the '+'-component of the current, the vertex factor in Eq.(4.1) is given by

$$\Gamma^+ = \sqrt{n_c}\sum_q e_q^2 \sum_{\lambda,\lambda'}\int_0^1 dx \int \frac{d^2\mathbf{k}_\perp}{16\pi^3}\psi_{P_S}(x_i,\mathbf{k}_\perp)\Big[\frac{\bar v_{\lambda'}(x_2,\mathbf{k}_\perp)}{\sqrt{x_2}}\not\epsilon\frac{u_\lambda(x_1,\mathbf{k}_\perp+\mathbf{q}_\perp)}{\sqrt{x_1}}$$
$$\times\frac{\bar u_\lambda(x_1,\mathbf{k}_\perp+\mathbf{q}_\perp)}{\sqrt{x_1}}\gamma^+\frac{u_\lambda(x_1,\mathbf{k}_\perp)}{\sqrt{x_1}}\frac{1}{\mathbf{q}_1^2-\frac{[(\mathbf{k}_\perp+\mathbf{q}_\perp)^2+m^2]}{x_1}-\frac{\mathbf{k}_\perp{}^2+m^2}{x_2}}+(1\leftrightarrow 2)\Big]. \tag{4.3}$$

Here, only anti-parallel helicities of constituents contribute to the integrations and our model wave function $\psi_{P_S}(x_i,\mathbf{k}_\perp)$ for anti-parallel helicities is given by

$$\psi_{P_S}(x_i,\mathbf{k}_\perp) = \frac{\pi}{2\beta^3}\Big(\frac{N_{P_S}}{2}\Big)^{1/2}\frac{(a_1a_2-\mathbf{k}_\perp{}^2)}{x_1x_2}\exp\Big(-\frac{\mathbf{k}_\perp{}^2+m^2}{8x(1-x)\beta^2}\Big). \tag{4.4}$$

A straightforward calculation for the transition $\pi^0 \to \gamma^*\gamma$ gives the following result

$$G_{\pi\gamma} = \sqrt{n_c}(q_u^2-q_d^2)I_2(m_M,m_{u(d)},\beta),$$
$$G_{\eta\gamma} = \sqrt{n_c}[X_\eta(q_u^2+q_d^2)I_2(m_M,m_{u(d)},\beta) - Y_\eta q_s^2\sqrt{2}I_2(m_M,m_s,\beta)],$$
$$G_{\eta'\gamma} = \sqrt{n_c}[X_{\eta'}(q_u^2+q_d^2)I_2(m_M,m_{u(d)},\beta) + Y_{\eta'}q_s^2\sqrt{2}I_2(m_M,m_s,\beta)], \tag{4.5}$$

where

$$I_2(m_M,m_q,\beta) = -\frac{\sqrt{N_{P_S}}}{\pi\beta}\int_0^1\frac{dx}{x}\exp\Big(-\frac{\tilde m^2}{2x(1-x)}\Big)\Big[2x(1-x)-\exp\Big(\frac{4\xi^2+\tilde m^2}{2x(1-x)}\Big)$$
$$\times(a_1a_2+\tilde m^2+4\xi^2)\int_\infty^1 dt\exp\Big(-\frac{4\xi^2+\tilde m^2}{2x(1-x)}t\Big)/t\Big]. \tag{4.6}$$

Using Eqs.(4.2)-(4.6), the decay widths for $P_S \to \gamma\gamma$ are obtained as

$$\Gamma(\pi^0\to\gamma\gamma) = 6.50\ \text{eV},$$
$$\Gamma(\eta\to\gamma\gamma) = 0.47[0.65]\ \text{keV},$$
$$\Gamma(\eta'\to\gamma\gamma) = 7.9[5.6]\ \text{keV}, \tag{4.7}$$

where the values for $\eta \to \gamma\gamma$ and $\eta' \to \gamma\gamma$ are obtained for the -10°[-23°] mixing scheme. The experimental data [47] are given by $\Gamma_{\pi\gamma}^{\rm exp} = 7.8 \pm 0.5$ eV, $\Gamma_{\eta\gamma}^{\rm exp} = 0.47 \pm 0.05$ keV and $\Gamma_{\eta'\gamma}^{\rm exp} = 4.3 \pm 0.6$ keV. The agreement of our results with the experimental data is not unreasonable. In Figs.6-8, the Q^2 dependence of the decay rate $\Gamma_{P_S\gamma}(Q^2)$ for $P_S = \pi^0, \eta$, and η' are shown and compared with the recent experimental data [23–25]. Our predictions for all of these processes are overall in a good agreement with the experimental data up to a rather large Q^2. In Table II, our predictions of the two photon decay widths for various β values are include.

V. SUMMARY AND DISCUSSION

In this paper, we have investigated the radiative decays of pseudoscalar(π, K, η, η'), vector(ρ, K^*, ω, ϕ) and axial vector(A_1) mesons as well as the form factors of ρ and A_1 mesons using a simple relativistic constituent quark model. The use of a spin averaged hadron mass in the lightcone quark model has of course a wide literature [7–12]. The kinematical constraints following from the proper Poincaré-group invariance has been studied in detail [10] and it is shown that our light-cone quark model wavefunctions given by Eq.(1.4) are Lorentz invariant. Also, in our method, each constituent is individually Melosh transformed and thus the orthogonality of the constructed meson wavefunctions is not spoiled by the Melosh transformation. Since we started from the orthogonal wave functions of pseudoscalar, vector and axial vector mesons, the constructed wavefunctions by the Melosh transformation are clearly orthogonal.

We summarized all of our predictions on the meson decay widths for various values of β ($\beta = 0.32, 0.34, 0.36, 0.38$) GeV in Table II. Remarkably, most of our predictions with the parameter β in this region are within the experimental errors. We have also investigated the sensitivity of our results by varying quark masses. For $\pm 10\%$ variation of the nonstrange quark masses, the decay width Γ and the transition charge radius $< r^2 >^{1/2}$ of the radiative meson decays change by 3-4% and 2-4%, respectively. Changing strange quark mass by $\pm 10\%$ for the process of $K^{*\pm} \to K^\pm\gamma$ yields 13-15% and 3-4% difference in the decay width and the transition charge radius, respectively.

Overall, our numerical results for all the meson radiative decays that we investigated in this model are remarkably in a good agreement with the experimental data. In our point of view, the success of this model hinges upon the simplicity of the light-cone vacuum. The

recent lattice QCD results [48] indicate that the mass difference between η' and pseudoscalar octet mesons due to the complicated nontrivial vacuum effect increases(or decreases) as the quark mass m_q decreases(or increases),*i.e.*, the effect of the topological charge contribution should be small as m_q increases. This makes us to believe that the complicated nontrivial vacuum effect can be traded off by the constituent quark masses. This may mean that there is a suppression of complicate zero mode contribution [49] from the light-cone vacuum in our model due to rather large constituent quark masses.

Our approach in this work was obviously to model the wavefuction rather than to model the potential. However, we have attempted to compare our results with various other available theoretical results [32-43] including the potential models and the QCD sum rules. At the very least, our results seem to be quite comparable with the results from modelling the potential. The results on the angular condition are also not drastically different from the result of the potential models (See Fig.1(a)). Furthermore, the agreement with the QCD sum rule results is not unreasonable. Therefore, the light-cone quark model presented here should be distinguished from the so called naive quark model. Our model has a predictive power and more experimentally measurable quantities should be calculated and compared with data. A particularly interesting prediction from our model is the branching ratio of $\phi \to \eta'\gamma$ estimated as 10^{-4} for the $\eta - \eta'$ mixing angle of -23°. For the mixing angle -10°, the estimation for this branching ratio is reduced by 60% from that of -23°. Thus, it will be very interesting to compare our results with the precise measurements envisioned at TJNAF.

VI. ACKNOWLEDGEMENT

This work was supported by the Department of Energy under the contract DE-FG05-90ER40589 and DE-FG02-96ER40947. The North Carolina Supercomputing Center is also acknowledged for the grant of Cray time. We wish to thank Professor Nathan Isgur for his careful reading of this paper and providing very useful informations on the mixing of η and η'.

APPENDIX A: SPIN AVERAGED MESON MASSES OF η, η', ω AND ϕ

Here, let's first list our flavor wave functions of the neutral pseudoscalar (η, η') and vector (ω, ϕ) nonet states to show explicitly how we obtained the values of spin averaged mass used in this paper;

$$\eta = \frac{1}{\sqrt{6}}(u\bar{u} + d\bar{d} - 2s\bar{s}), \tag{A1}$$

$$\eta' = \frac{1}{\sqrt{3}}(u\bar{u} + d\bar{d} + s\bar{s}), \tag{A2}$$

$$\omega = \frac{1}{\sqrt{2}}(u\bar{u} + d\bar{d}), \tag{A3}$$

$$\phi = s\bar{s}. \tag{A4}$$

For ideally mixed isocalar and isovector mesons, we take the flavor wave function as

$$\begin{aligned} \chi_{ns}^{P_S(V)} &= \frac{1}{\sqrt{2}}(u\bar{u} + d\bar{d}), \\ \chi_s^{P_S(V)} &= s\bar{s}, \end{aligned} \tag{A5}$$

where $P_S(V)$ denotes pseudoscalar(vector) meson states. In terms of this basis, the neutral meson nonet states are given by

$$\begin{aligned} \eta_1 &= \sqrt{\frac{2}{3}}\chi_{ns}^{P_S} + \sqrt{\frac{1}{3}}\chi_s^{P_S}, \quad \omega_1 = \sqrt{\frac{2}{3}}\omega + \sqrt{\frac{1}{3}}\phi, \\ \eta_8 &= \sqrt{\frac{1}{3}}\chi_{ns}^{P_S} - \sqrt{\frac{2}{3}}\chi_s^{P_S}, \quad \omega_8 = \sqrt{\frac{1}{3}}\omega - \sqrt{\frac{2}{3}}\phi \end{aligned} \tag{A6}$$

where $\eta = \eta_8$, $\eta' = \eta_1$, $\omega = \chi_{ns}^V$ and $\phi = \chi_s^V$. We define the spin averaged masses $\bar{M}$ of χ_{ns} and χ_s as follows;

$$\begin{aligned} \bar{M}_{ns} &= \frac{1}{4}M_{ns}^{P_S} + \frac{3}{4}M_{ns}^V, \\ \bar{M}_s &= \frac{1}{4}M_s^{P_S} + \frac{3}{4}M_s^V. \end{aligned} \tag{A7}$$

Using Eqs.(A3),(A4),(A5) and (A6), we assign

$$\begin{aligned} M_\eta^{exp} &= \frac{1}{3}M_{ns}^{P_S} + \frac{2}{3}M_s^{P_S}, \\ M_{\eta'}^{exp} &= \frac{2}{3}M_{ns}^{P_S} + \frac{1}{3}M_s^{P_S}, \\ M_\omega^{exp} &= M_{ns}^V, \\ M_\phi^{exp} &= M_s^V. \end{aligned} \tag{A8}$$

Then, we obtain the following spin averaged masses of η and η';

$$\bar{M}_\eta = \frac{1}{3}\bar{M}_{n\bar{n}} + \frac{2}{3}\bar{M}_{s\bar{s}} = 842\text{MeV}, \tag{A9}$$

$$\bar{M}_{\eta'} = \frac{2}{3}\bar{M}_{n\bar{n}} + \frac{1}{3}\bar{M}_{s\bar{s}} = 885\text{MeV}. \tag{A10}$$

Likewise, from Eq.(A6), we obtain

$$\bar{M}_{\omega_1} = \frac{2}{3}\bar{M}_\omega + \frac{1}{3}\bar{M}_\phi, \tag{A11}$$

$$\bar{M}_{\omega_8} = \frac{1}{3}\bar{M}_\omega + \frac{2}{3}\bar{M}_\phi. \tag{A12}$$

Using $\bar{M}_\eta = \bar{M}_{\omega_8}$ and $\bar{M}_{\eta'} = \bar{M}_{\omega_1}$, we can then evaluate the spin averaged masses of ω and ϕ as $\bar{M}_\omega = 928$ MeV and $\bar{M}_\phi = 799$ MeV, respectively.

To calculate the spin averaged meson masses depending on the schemes of flavor mixing, let's consider the "perfect mixing"($\theta_{SU(3)} = -10^o$) $\tilde{\eta}$ and $\tilde{\eta}'$ states defined by [19,20],

$$\tilde{\eta} = \frac{1}{\sqrt{2}}(\chi^{Ps}_{n\bar{n}} - \chi^{Ps}_{s\bar{s}}), \quad \tilde{\eta}' = \frac{1}{\sqrt{2}}(\chi^{Ps}_{n\bar{n}} + \chi^{Ps}_{s\bar{s}}). \tag{A13}$$

Using Eqs.(A13) and Eq.(A6), we obtain

$$\eta_1 = \frac{\sqrt{2}-1}{\sqrt{6}}\tilde{\eta} + \frac{\sqrt{2}+1}{\sqrt{6}}\tilde{\eta}',$$

$$\eta_8 = \frac{1+\sqrt{2}}{\sqrt{6}}\tilde{\eta} + \frac{1-\sqrt{2}}{\sqrt{6}}\tilde{\eta}'. \tag{A14}$$

Thus, the spin averaged masses $\bar{m}$ of the $\tilde{\eta}$ and $\tilde{\eta}'$ in "perfect mixing" scheme are related to $\bar{M}_\eta$ and $\bar{M}_{\eta'}$ calculated in our scheme (see Eqs.(A9) and (A10)),respectively, as follows;

$$\bar{M}_{\eta'} = \frac{(\sqrt{2}-1)^2}{6}\bar{m}_{\tilde{\eta}} + \frac{(\sqrt{2}+1)^2}{6}\bar{m}_{\tilde{\eta}'},$$

$$\bar{M}_\eta = \frac{(\sqrt{2}+1)^2}{6}\bar{m}_{\tilde{\eta}} + \frac{(\sqrt{2}-1)^2}{6}\bar{m}_{\tilde{\eta}'}. \tag{A15}$$

From Eq.(A15), the spin averaged masses for the "perfect mixing" states are given by $\bar{m}_{\tilde{\eta}} =$ 843 MeV and $\bar{m}_{\tilde{\eta}'} =$ 884 MeV, respectively. Using the same method in the above, for the $\theta_{SU(3)} = -23^o$ mixing scheme, we obtain the following spin averaged meson masses: $m_\eta = 838$ MeV and $m_{\eta'} = 873$ MeV, respectively.

APPENDIX B: THE ELECTROMAGNETIC DECAY WIDTH $\Gamma(A \to B + \gamma)$

In this appendix, we derive the decay widths of $A \to B + \gamma$ ($A = \rho, K^*, \omega, \phi$, and $B = \pi, K, \eta, \eta'$) and $A_1 \to \pi + \gamma$.

Consider the electromagnetic decay process $A \to B + \gamma$. If the masses of A and B mesons are given by m_A and m_B, respectively, then the decay rate $\Gamma(A \to B + \gamma)$ in the rest frame of A is given by ($\hbar = c = 1$);

$$\Gamma(A \to B + \gamma) = \frac{1}{(2\pi)^6}\frac{S}{2m_A}\int \frac{d^3\mathbf{p}_B}{2E_B}\frac{d^3\mathbf{p}_\gamma}{2E_\gamma}|\mathcal{M}|^2(2\pi)^4\delta^3(\mathbf{p}_B + \mathbf{p}_\gamma)\delta(m_A - E_B - E_\gamma), \tag{B1}$$

where $S = 1/j!$ for each group of j identical particles in the final states. Here, $\mathcal{M}$ is the transition matrix element defined by

$$\mathcal{M} = \epsilon^*_\mu(\lambda_\gamma) < B(P')|J^\mu|A(P,\lambda) > . \tag{B2}$$

To allow decays to all possible spin configurations, we consider the replacement

$$|\mathcal{M}|^2 \to \overline{|\mathcal{M}|}^2 \equiv \frac{1}{2S_A+1}\sum_{\lambda_\gamma=\pm1}|\mathcal{M}|^2, \tag{B3}$$

where S_A is the spin of particle A and λ_γ corresponds to the state of transverse polarization of the emitted photon. The above replacement means the average over the initial spin and the sum over the helicities of the emitted photon. Then, from Eq.(B1), we get

$$\Gamma(A \to B + C) = \frac{S}{2(4\pi)^2 m_A}\frac{1}{2S_A+1}\int |\mathbf{p}_B|^2 d|\mathbf{p}_B| d\Omega \frac{\delta(m_A - \sqrt{m_B^2 + \mathbf{p}_B^2} - |\mathbf{p}_B|)}{|\mathbf{p}_B|\sqrt{m_B^2 + \mathbf{p}_B^2}} \times \sum_{\lambda_\gamma=\pm1}|\mathcal{M}|^2. \tag{B4}$$

If we let $|\mathbf{p}_B| = \rho$ and $E \equiv \sqrt{m_B^2 + \rho^2} + \rho$, then

$$\Gamma(A \to B + \gamma) = \frac{S}{8\pi m_A}\frac{1}{2S_A+1}\int_{m_B}^\infty dE\frac{\rho}{E}\delta(m_A - E)\sum_{\lambda_\gamma=\pm1}|\mathcal{M}|^2, \tag{B5}$$

Therefore, we get

$$\Gamma(A \to B + \gamma) = \frac{S}{8\pi m_A^2}\frac{\rho_0}{2S_A+1}\sum_{\lambda_\gamma=\pm1}|\mathcal{M}|^2, \tag{B6}$$

where

$$S = 1 \quad \text{if} \quad \text{B} \neq \gamma$$

$$S = \frac{1}{2} \quad \text{if} \quad \text{B} = \gamma. \tag{B7}$$

Here, ρ_0 is the value of ρ when $E = m_A$, *i.e.*, $\rho_0 = (m_A^2 - m_B^2)/2m_A$. In the rest frame of A,*i.e.*, $P_A = (m_A, \vec{0})$,$P'_B = (m_B, \mathbf{p}_B)$ and $P_\gamma = (|\mathbf{p}_B|, -\mathbf{p}_B)$, the invariant amplitude square is given by

$$\sum_{\lambda_\gamma=\pm1}|\mathcal{M}|^2 = \sum_{\lambda_\gamma=\pm1}|eG_{AB}(Q^2)\varepsilon^{\mu\nu\alpha\beta}\epsilon^*_\mu(\lambda_\gamma)\epsilon_\nu(P,\lambda)P'_\alpha P_\beta|^2$$
$$= e^2|G_{AB}(Q^2)|^2 2|\varepsilon^{12\alpha\beta}P'_\alpha P_\beta|^2$$
$$= e^2|G_{AB}(Q^2)|^2 2m_A^2\mathbf{p}_B^2$$
$$= \frac{(m_A^2-m_B^2)^2}{2}e^2|G_{AB}(Q^2)|^2. \qquad \text{(B8)}$$

Therefore, we get the following decay width $\Gamma(A\to B+\gamma)$

$$\Gamma(A\to B+\gamma) = \frac{\alpha}{2S_A+1}|G_{AB}(0)|^2(\frac{m_A^2-m_B^2}{2m_A})^3, \qquad \text{(B9)}$$

where $\alpha(=e^2/4\pi)$ is the fine structure constant.

The decay width of $A_1\to\pi\gamma$ can be calculated in the same manner using our definition of the transition matrix element given by Eq.(3.2) as follows;

$$\sum_{\lambda_\gamma=\pm1}|\mathcal{M}|^2 = |\epsilon^*_\mu(\lambda_\gamma)<\pi(P')|J^\mu|A_1(P,\lambda)>|^2$$
$$= 2|e\frac{G_1(Q^2)}{m_{A_1}}(P_{A_1}+P'_\pi)\cdot P_\gamma|^2$$
$$= 2|e\frac{G_1(Q^2)}{m_{A_1}}|\mathbf{p}_\pi|(m_{A_1}+m_\pi+|\mathbf{p}_\pi|)|^2$$
$$= 2e^2|\frac{G_1(Q^2)}{m_{A_1}}|^2(2m_{A_1}\mathbf{p}_\pi)^2, \qquad \text{(B10)}$$

and the result is given by

$$\Gamma(A_1\to\pi\gamma) = \frac{4\alpha}{3}|\frac{G_1(0)}{m_{A_1}}|^2(\frac{m_{A_1}^2-m_\pi^2}{2m_{A_1}})^3. \qquad \text{(B11)}$$

REFERENCES

[1] V.L.Chernyak and I.R.Zhitnitsky, Phys.Rep.**112**, 1738(1984).

[2] S.Narison, Phys.Lett.B **224**, 184(1989).

[3] A.V.Radyushkin, presented at 2nd European Workshop on Hadronic Physics with Electrons Beyond 10-Gev,Dourdan,France,1990.

[4] S.Gottlieb and A.S.Kronfeld, Phys.Rev.Lett. **55**, 2531(1985).

[5] T.A.DeGrand and R.D.Loft, Phys.Rev.D **38**, 954(1988).

[6] D.Daniel,R.Gupta,and D.G.Richards, Phys.Rev.D**43**, 3715(1991).

[7] C.-R.Ji and S.R.Cotanch, Phys.Rev.D **41**, 2319(1990).

[8] C.-R.Ji, P.L.Chung, and S.R.Cotanch, Phys.Rev.D **45**, 4214(1992).

[9] Z.Dziembowski and L.Mankiewicz, Phys.Rev.Lett.**58**, 2175(1987); Z.Dziembowski, Phys.Rev.D **37**, 2030(1988).

[10] Z.Dziembowski, Phys.Rev.D **37**, 768(1988); **37**, 778(1988).

[11] J.Bienkowska, Z.Dziembowski, and H.J.Weber, Phys.Rev. Lett. **59**, 177(1987); H.J.Weber, Phys.Lett.B **287**, 14(1992); Phys.Rev.D **41**, 2201(1992); Ann.Phys.(N.Y.) **177**, 38(1987); **207**, 417(1991).

[12] X.Guo and T.Huang, Phys.Rev.D **43**, 2931(1991).

[13] G.P.Lepage, S.J.Brodsky, T.Huang, and P.Mackenzie, in *Particle and Fields 2*, edited by A.Z.Capri and A.N.Kamal(Plenum, New York,1983),p.83.

[14] C.-R.Ji and Y.Surya, Phys.Rev. D **46**, 3565(1992).

[15] D.E.Soper, ph.D. Thesis, SLAC Report No. **137**(1971).

[16] C.Hayne and N.Isgur, Phys.Rev.D **25**, 1944(1982).

[17] H.J.Melosh, Phys.Rev.D **9**, 1095(1974); L.A.Kondratyuk and M.V.Terentyev, Sov.J.Nucl.Phys. **31**, 561(1983).

[18] N.Isgur, in *The New Aspect of Subnuclear Physics*, editted by A.Zichichi (Plenum, New York, 1980), p.107.

[19] N.Isgur, Phys.Rev.D **12**, 3770(1975).

[20] Stephen Godfrey and Nathan Isgur, Phys.Rev.D **32**, 189(1985).

[21] Review of Particle Physics, Phys.Rev.D **54**, 99(1996).

[22] B.L.Ioffe and A.V.Smilga, Nucl.Phys.B **216**, 373(1983); Phys.Lett.B **114**, 353(1982).

[23] CELLO coll., H.-J.Behrend et al., Z.Phys.C **49**, 401(1991).

[24] CELLO coll., V.Savinov et al., these proceedings.

[25] TPC/2γ coll., H.Aihara et al., Phys.Rev.Lett.**64**, 172(1990).

[26] S.D.Drell and T.M.Yan, Phys.Rev.Lett. **24**, 181(1970).

[27] R.G.Arnold, C.E.Carlson, and F.Gross, Phys.Rev.C **21**, 1426(1980)

[28] G.P.Lepage and S.J.Brodsky, Phys.Rev.D **22**, 2157(1980).

[29] P.L.Chung, F.Coester, B.D.Keister and W.N.Polyzou, Phys.Rev.C **37**,2000(1988).

[30] C.E.Carlson and F.Gross, Phys.Rev.Lett. **53**, 127(1984).

[31] S.J.Brodsky and J.R.Hiller, Phys.Rev.D **46**, 2141(1992).

[32] I.L.Grach and L.A.Kondratyuk, Sov.J.Nucl.Phys. **39**, 198(1984).

[33] B.D.Keister, Phys.Rev.C **49**, 1500(1994).

[34] F.Cardarelli *et al.*, Phys.Lett.B **349**, 393(1995) ;**359**, 1(1995).

[35] A.S.Bagdasaryan and S.V.Esaybegyan, Sov.J.Nucl.Phys.**42**, 278(1985).

[36] H.Ito and F. Gross, Phys.Rev.Lett. **71** 2555(1993).

[37] I.G.Aznauryan and K.A.Oganessyan, Phys.Lett.B **249**, 309(1990).

[38] R.I.Dzhelyadin *et al.*, Phys.Lett. **102B**, 296(1981).

[39] C.R.Münz et al., Phys.Lett.C **52**, 2110(1995).

[40] V.M.Braun and I.E.Filyanov, Z.Phys.C **44**, 157(1989); ibid. C **48**, 239(1990).

[41] V.M.Belyaev, Z.Phys.C **65**, 93(1995).

[42] J.Babcock and J.L.Rosner, Phys.ReV.D **14**, 1286(1976).

[43] J.L.Rosner, Phys.Rev.D **23**, 1127(1981).

[44] M.Zielinski et al., Phys.Rev.Lett. **52**, 1195(1984).

[45] M.Zielinski, Phys.Rev.Lett. **58**, 2002(1987).

[46] F.G.Cao, T.Huan, and B.Q.Ma, Phys.Rev.D **53**, 6582(1996).

[47] Particle Data Group, Phys.Rev.D **50**, 1173(1994).

[48] Y.Kuramashi, M.Fukugita et al., Phys.Rev.Lett.**72**, 3448(1994).

[49] C.-R.Ji and S.J.Rey, Phys.Rev.D **53**, 5815(1996).

FIGURES

Fig.1(a). $\Delta(Q^2)$ testing the angular condition is shown as a function of Q^2. The solid lines are our results with $\beta = 0.32$ and 0.36 GeV. For comparison, we include various choices of the wave function w^ρ introduced by Godfrey and Isgur(GI) in Ref. [34]. The dashed, dotted and dashed-dotted lines correspond to w_{si}(spin-independent part), w_{GI}(OGE + linear confining term) and w_{conf}(linear confinging term), respectively.

Fig.1(b). The form factors of ρ meson with parameter $\beta = 0.36$ GeV. The solid, dotted, and dashed lines correspond to $F_C(Q^2)$,$F_M(Q^2)$ and $F_Q(Q^2)$, respectively. The dashed-dotted line is the result of non-relativistic limit of $F_C(Q^2)$ by turning off the Melosh transformation.

Fig.1(c). The form factors, $G_1 = F_1$, $G_2 = F_2 - F_1$ and $G_3 = F_3/2$, of ρ meson are compared with the results of QCD sum rules [22]. The dotted, dashed and dashed-dotted lines correspond to G_1, G_2, and G_3 of Ref. [22]

Fig.2(a). The form factors of A_1 meson with the parameter $\beta = 0.36$ GeV. The solid, dotted, and dashed lines correspond to F_C, F_M, and F_Q, respectively. The quantity $|\Delta(Q^2)|$ is shown as dashed-dotted line.

Fig.2(b). The form factors, $G_1 = F_1$, $G_2 = F_2 - F_1$ and $G_3 = F_3/2$, of A_1 meson are compared with the result of QCD sum rules [22]. The solid, dotted, and dashed lines are our predictions of G_1, $G_2/2$, and G_3, respectively. The QCD sum-rule results are $G_1(Q^2)$(long dashed line) and $G_2(Q^2)/2$(dashed-dotted line).

Fig.3(a). The transition form factor of $\rho^+ \to \pi^+\gamma^*$ multiplied by Q^4 is shown as a function of Q^2. The solid lines are our results with $\beta = 0.32$ and 0.36 GeV. The dotted line, dashed, and dashed-dotted lines correspond to the results obtained using w_{GI} in Ref. [34], the BS approach of Ref. [36] and the predictions of VDM model with $G_{\rho\pi} = 1/(1 + Q^2/M_\rho^2)$.

Fig.3(b). The normalized transition form factor of $\omega \to \pi\gamma^*$. Our result with $\beta = 0.36$ GeV(solid line) is compared with VDM with $G_{\omega\pi} = 1/(1 + Q^2/M_\rho^2)$ and the pole fit of the experimental data(dotted line) [38].

Fig.4. The normalized form factors of $K^{*+} \to K^+\gamma^*$(solid line) and $K^0 \to K^0\gamma^*$(dotted line) transitions with the parameter $\beta = 0.36$ GeV. The dotted and dashed lines correspond to charged and neutral vector kaon transition form factors by Ref. [39]. The dashed-dotted line corresponds to the VDM prediction.

Fig.5. The form factors of $A_1^+ \to \pi^+\gamma^*$ transition with the parameter $\beta = 0.36$ GeV. $G_1(Q^2)$ and $G_2(Q^2)/10$ of our results are represented by the solid and dashed lines, respectively.For comparison, we show also the QCD sum-rule results:$G_1(Q^2)$(dotted-line) and $G_2(Q^2)/10$(dotted-dashed line).

Fig.6. The decay rate for $\pi^0 \to \gamma^*\gamma$ transition with the parameter $\beta = 0.36$ GeV. Data are taken from Ref. [23,24].

Fig.7. The decay rate for $\eta \to \gamma^*\gamma$ transition with the parameter $\beta = 0.36$ GeV. The solid and dotted lines correspond to the $\theta_{SU(3)} = -10^\circ$ and -23° mixing schemes, respectively. Data are taken from Ref. [23-25].

Fig.8. The decay rate for $\eta' \to \gamma^*\gamma$ transition with the parameter $\beta = 0.36$ GeV. The solid and dotted lines correspond to the $\theta_{SU(3)} = -10^\circ$ and -23° mixing schemes, respectively. Data are taken from Ref. [23-25].

TABLES

TABLE I. Three different mixing schemes for η and η' and the corresponding spin averaged masses.

$\theta_{SU(3)}$	X_η	Y_η	$X_{\eta'}$	$Y_{\eta'}$	m_η[MeV]	$m_{\eta'}$[MeV]
0°	$\sqrt{1/3}$	$\sqrt{2/3}$	$\sqrt{2/3}$	$\sqrt{1/3}$	842	885
-10°	$\sqrt{1/2}$	$\sqrt{1/2}$	$\sqrt{1/2}$	$\sqrt{1/2}$	843	884
-23°	0.85	0.53	0.53	0.85	834	873

TABLE II. Decay widths for $V \to P_S\gamma$, $P_S \to V\gamma$, $A_1 \to \pi\gamma$ and $P_S \to 2\gamma$ with $P_S = \pi, K, \eta, \eta'$ and $V = \rho, K^*, \omega, \phi$ for various model parameters β

β[GeV]	0.32	0.34	0.36	0.38	ST[a]	Experiment[b]
$\Gamma(\rho^\pm \to \pi^\pm\gamma)$	78	73	69	64		60 ± 8[keV][c]
$\Gamma(\omega \to \pi\gamma)$	775	742	708	674		717 ± 51
$\Gamma(K^{*\pm} \to K^\pm\gamma)$	60	57	53	50		50 ± 5
$\Gamma(K^{*0} \to K^0\gamma)$	134	128	122	116		117 ± 10
$\Gamma(\rho \to \eta\gamma)$[d]	66[77]	60[70]	56[65]	51[60]	40	58 ± 10
$\Gamma(\omega \to \eta\gamma)$	7.4[8.5]	6.9[7.9]	6.4[7.4]	6.0[6.8]	4.6	7.0 ± 1.8
$\Gamma(\eta' \to \rho\gamma)$	137[89]	126[80]	117[72]	108[66]	144	61 ± 8
$\Gamma(\eta' \to \omega\gamma)$	11.2[7.3]	10.4[6.6]	9.7[6.0]	9.1[5.6]	12.0	5.9 ± 0.9
$\Gamma(\phi \to \eta\gamma)$	54[40]	58[42]	61[45]	65[47]	71	56.9 ± 2.9
$\Gamma(\phi \to \eta'\gamma)$	0.26[0.43]	0.27[0.44]	0.28[0.45]	0.29[0.46]	0.23	< 1.8
$\Gamma(A_1 \to \pi\gamma)$	620	664	705	742		640 ± 246 [44,45]
$\Gamma(\pi^0 \to 2\gamma)$	7.58	7.06	6.50	5.91		7.8 ± 0.5[eV]
$\Gamma(\eta \to 2\gamma)$	0.61[0.78]	0.53[0.71]	0.47[0.65]	0.42[0.58]	0.44	0.47 ± 0.05
$\Gamma(\eta' \to 2\gamma)$	8.8[6.5]	8.3[6.1]	7.9[5.6]	7.3[5.1]	9.0	4.3 ± 0.6

[a] ST = standard mixing($\theta_{SU(3)} = 0°$) for $\beta = 0.36$ GeV.

[b] From Ref. [47], unless otherwise noted.

[c] The unit of decay width is [keV], unless otherwise noted.

[d] The values are the result from $\theta_{SU(3)} = -10°[-23°]$ mixing scheme.

Fig.1(a)

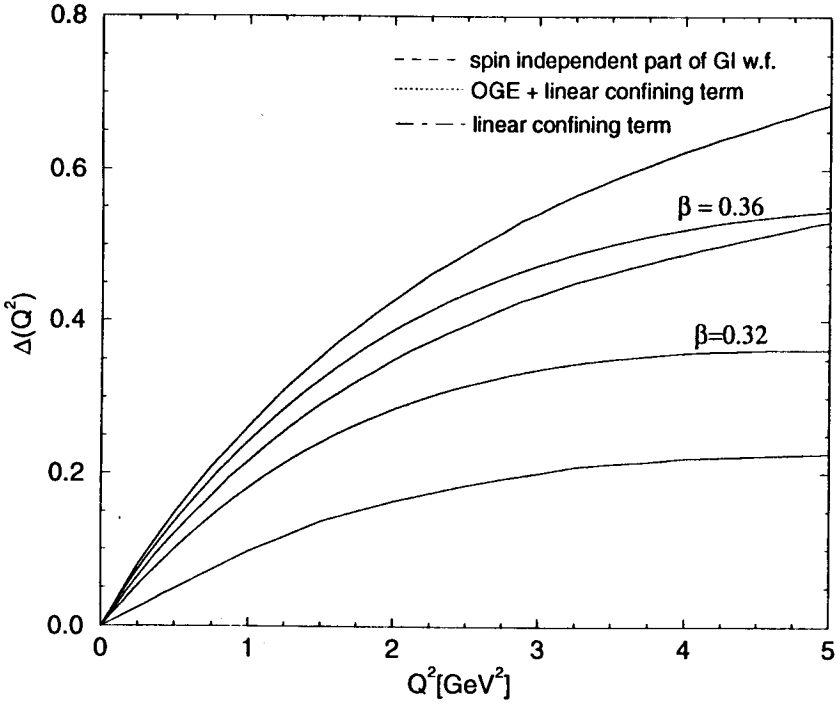
spin independent part of GI w.f.
OGE + linear confining term
linear confining term
β = 0.36
β=0.32
Δ(Q²)
Q²[GeV²]
0.0
0.2
0.4
0.6
0.8
0
1
2
3
4
5

Fig.1(b)

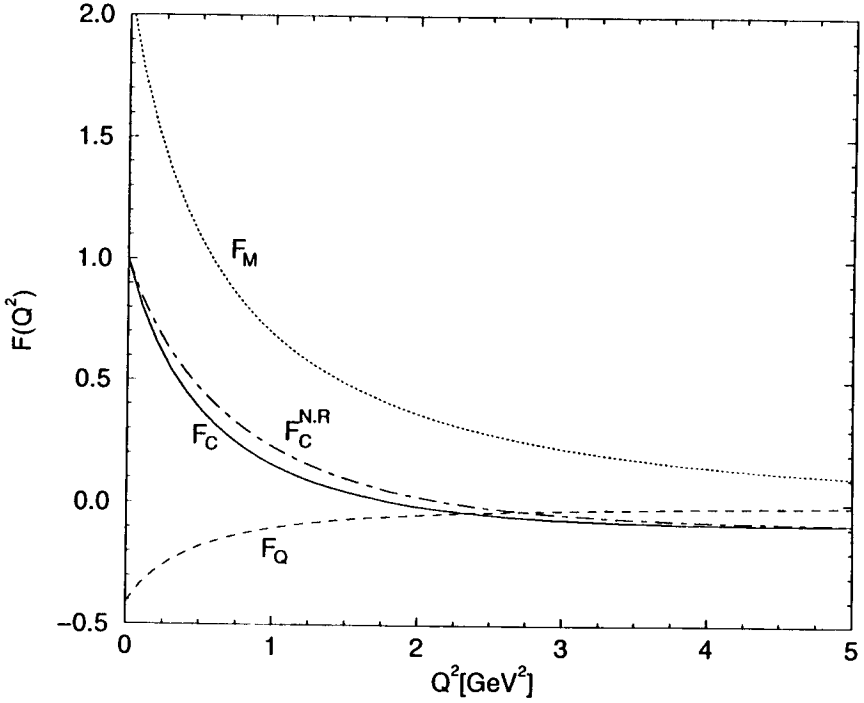
F_M
F_C
F_C^N.R
F_Q
F(Q²)
Q²[GeV²]
2.0
1.5
1.0
0.5
0.0
−0.5
0
1
2
3
4
5

Fig.1(c)

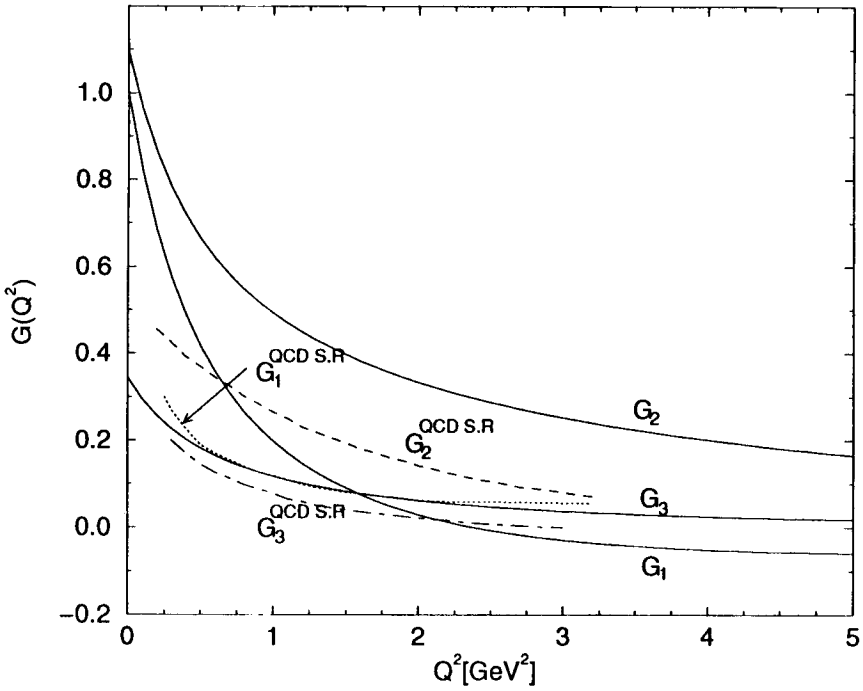
G(Q²)
Q²[GeV²]
G1 QCD S.R
G2 QCD S.R
G3 QCD S.R
G1
G2
G3

Fig.2(a)

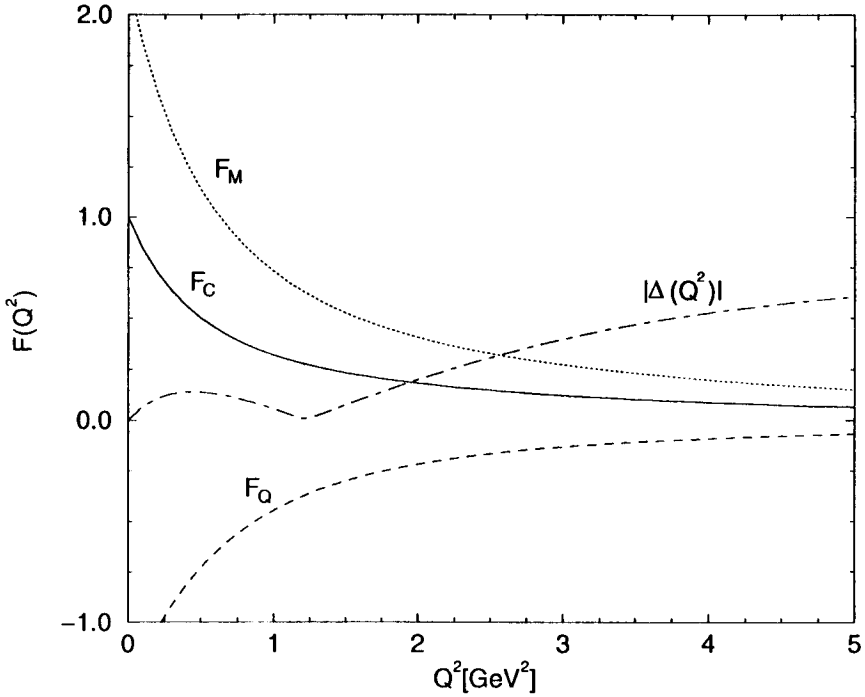
F(Q²)
Q²[GeV²]
FM
FC
FQ
|Δ(Q²)|

Fig.2(b)

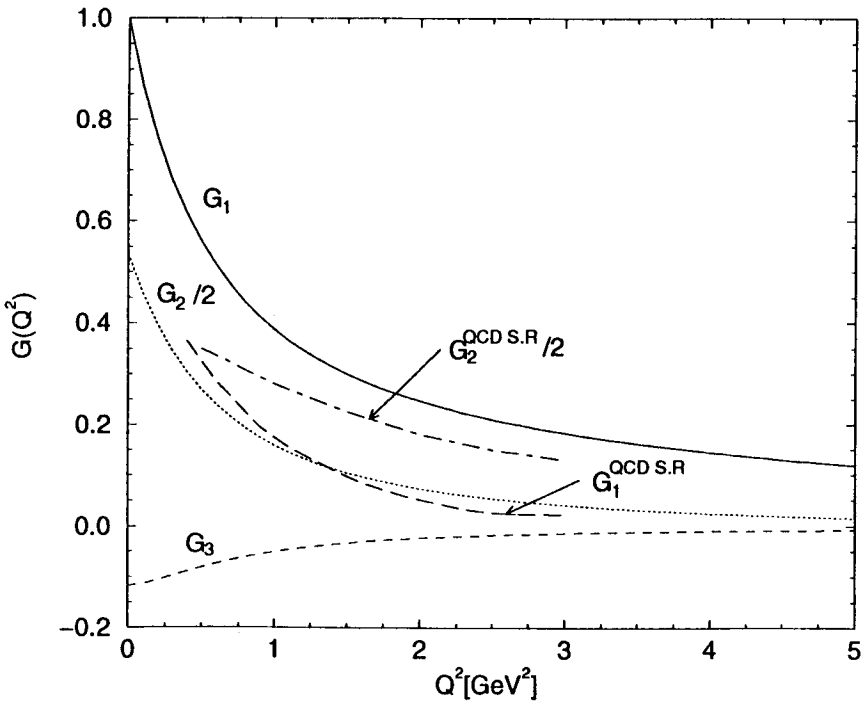
1.0
0.8
0.6
0.4
0.2
0.0
-0.2
0
1
2
3
4
5
G(Q²)
Q²[GeV²]
G₁
G₂ /2
G₂^QCD S.R /2
G₁^QCD S.R
G₃

Fig.3(a)

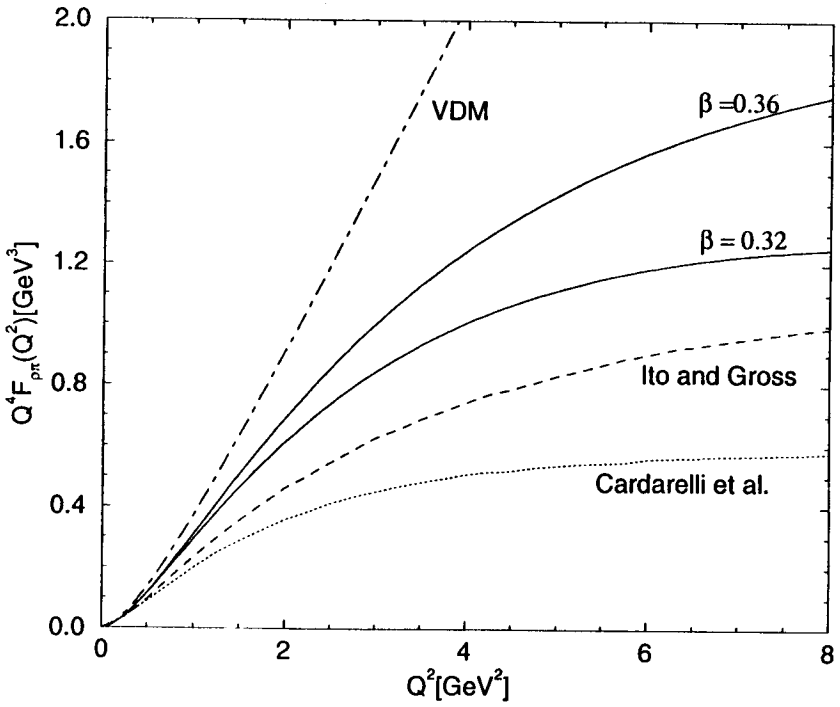
2.0
1.6
1.2
0.8
0.4
0.0
0
2
4
6
8
Q⁴F_pπ(Q²)[GeV³]
Q²[GeV²]
VDM
β =0.36
β = 0.32
Ito and Gross
Cardarelli et al.

Fig.3(b)

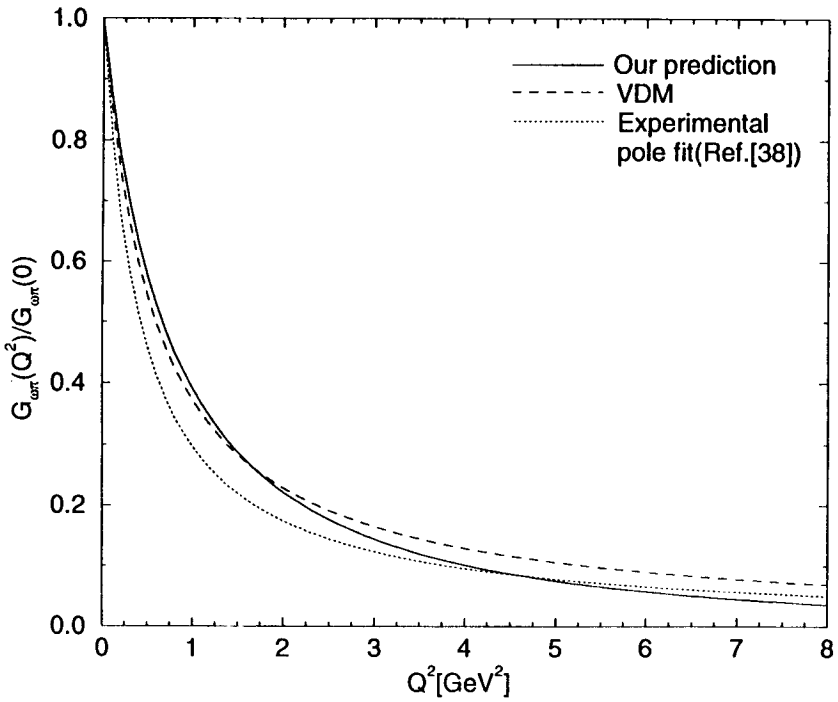
Our prediction
VDM
Experimental
pole fit(Ref.[38])
$G_{\omega\pi}(Q^2)/G_{\omega\pi}(0)$
Q^2[GeV^2]

Fig.4

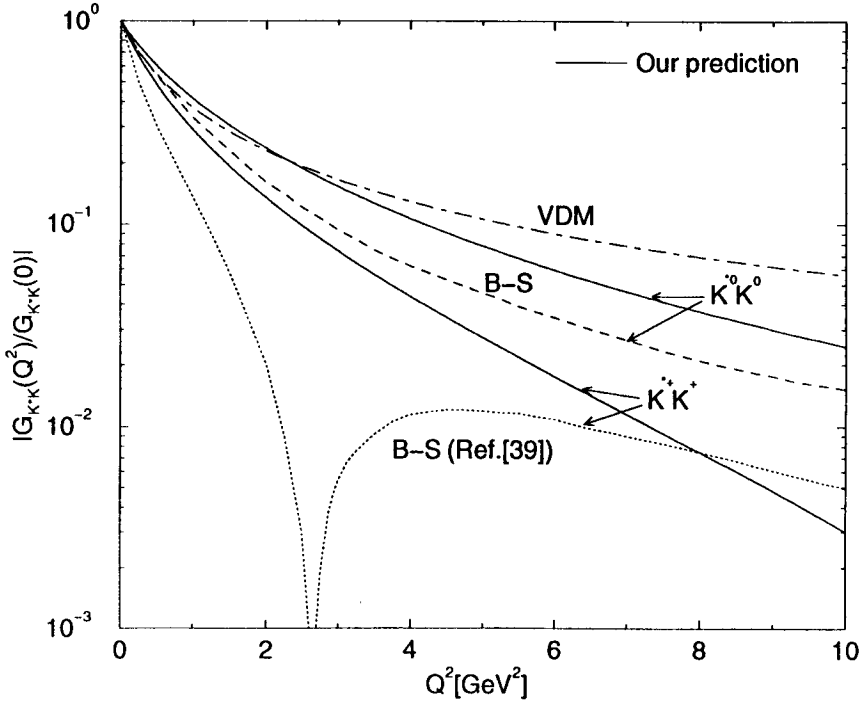
Our prediction
VDM
B–S
$K^{*0}K^{0}$
$K^{*+}K^{+}$
B–S (Ref.[39])
$|G_{K^*K}(Q^2)/G_{K^*K}(0)|$
Q^2[GeV^2]

Fig.5

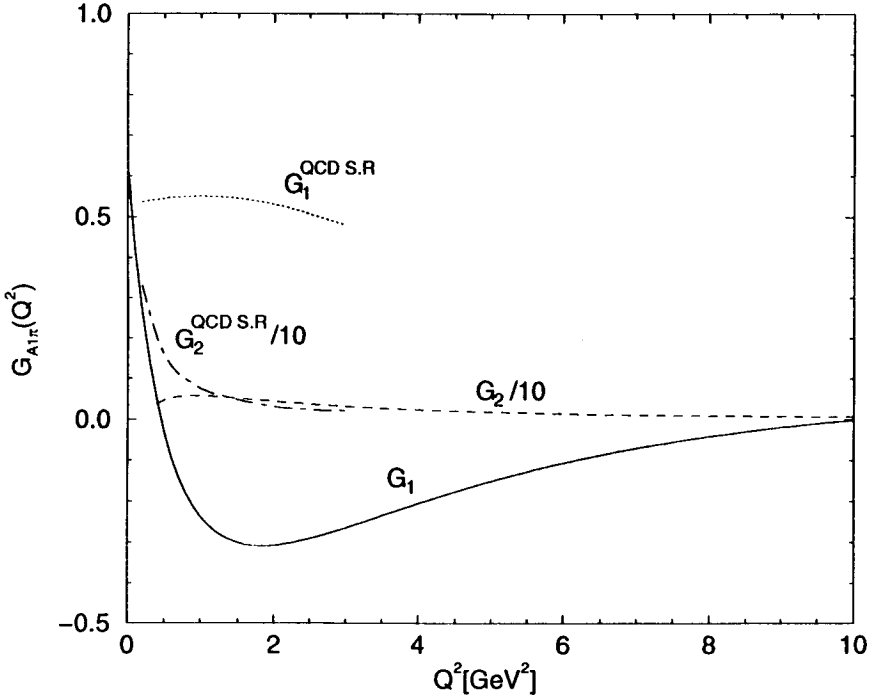
1.0
0.5
0.0
−0.5
0
2
4
6
8
10
$G_{A1\pi}(Q^2)$
$Q^2[GeV^2]$
$G_1^{QCD\ S.R}$
$G_2^{QCD\ S.R}/10$
$G_2/10$
G_1

Fig.6

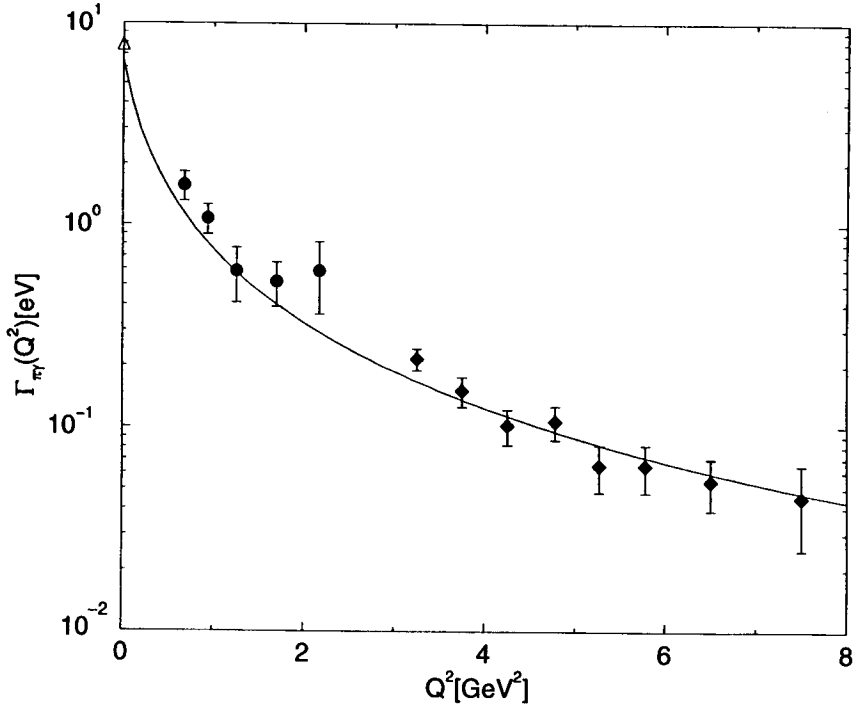
10^1
10^0
10^{-1}
10^{-2}
0
2
4
6
8
$\Gamma_{\pi\gamma}(Q^2)[eV]$
$Q^2[GeV^2]$

Fig.7

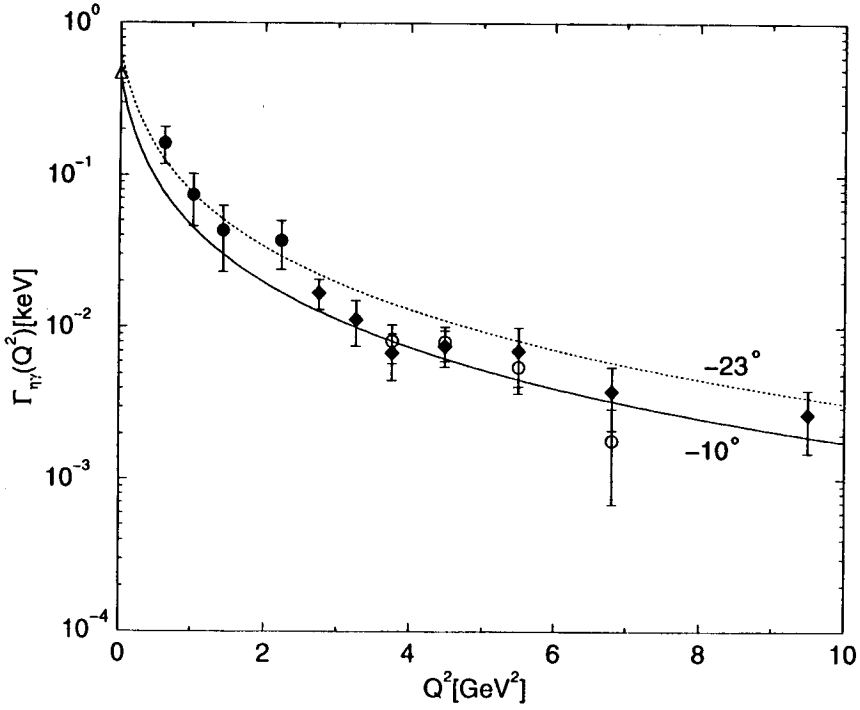
10^0
10^{-1}
10^{-2}
10^{-3}
10^{-4}
$\Gamma_{\eta\gamma^*}(Q^2)$[keV]
0
2
4
6
8
10
Q^2[GeV^2]
-23°
-10°

Fig.8

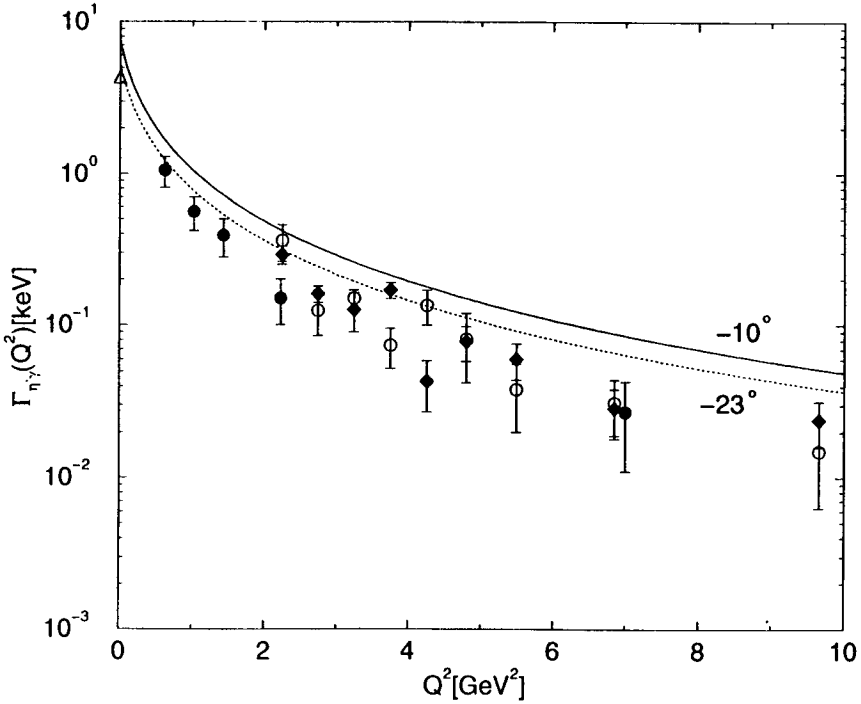
10^1
10^0
10^{-1}
10^{-2}
10^{-3}
$\Gamma_{\eta'\gamma^*}(Q^2)$[keV]
0
2
4
6
8
10
Q^2[GeV^2]
-10°
-23°